

# Boundary lubrication additives for aluminium: A journey from nano to macrotribology

D. Devaprakasam, O.P. Khatri, N. Shankar, S.K. Biswas\*

*Department of Mechanical Engineering, Indian Institute of Science, Bangalore 560 012, India*

Available online 24 August 2005

## Abstract

The tribology of two potential additive molecules for aluminium has been studied in the self assembled monolayer state at low loads ( $10^{-9}$ – $10^{-2}$  N) and in dispersion state in *n*-hexadecane at high load (60 N). The two additive molecules are 1H, 1H, 2H, 2H-perfluorooctyltrichlorosilane (FOTS), which has a rigid rod-like helical structure and octadecyltrichlorosilane (OTS), which has a zigzag backbone configuration. The adhesion, friction and wear performance have been investigated. Molecular conformational order and stiffness were found to play major roles in frictional dissipation and wear resistance, recorded in a nanotribometer and a pin-on-disc machine, while for very low load measurements (LFM), adhesion was found to have a significant role on friction along with molecular entropy.

© 2005 Published by Elsevier Ltd.

*Keywords:* Atomic force microscopy; Fourier transform infrared spectroscopy; Macrotribology

## 1. Introduction

Aluminium and magnesium are likely to make major inroads as engine materials for mass manufactured cars in the next decade or so. A search towards this is therefore, an objective to optimization of engine tribology, will play an important role. A unique combination of optimum microstructure and optimum interfaces, which are protective, efficient in transmission and minimize dissipation losses needs to be evolved. A search for additives, which can generate such interfaces for light metals, normally covered with persistent layers of oxides and hydroxides, has acquired a renewed impetus. We look to a new generation of commercially available additives, presently considered [1–6] for protection of semiconductor silicon surfaces and components in electronic packaging, micro electro-mechanical systems and information storage, for possible use as boundary lubrication additives for aluminium-based components used in moving machinery. These are organosilanes, which adhere to the aluminium substrate through oxygen atoms by self-assembled process [7,8].

Many potential applications of self-assembled monolayers (SAM) have inspired extensive scrutiny of their tribological properties. High temperatures and extreme pressure are likely to remove these monolayers; we thus limit our outlook to relatively mild conditions. Properties of interest are adhesion, friction and wear [9]. Polar functionality of the terminal group, molecular entropy or conformational order influenced by intermolecular Van der Waals forces, lateral polymerization, steric hindrance, structure and stiffness of the backbone and chemical/physical affinity of the head group to the substrate are relevant parameters which may influence tribology. In this the aggregate functionality near the surface is influenced by molecular entropy while external variables such as pressure, temperature and the medium and its polarity intervene through the above parameters to fix the specificities of tribological interaction. Given this generality, what is, however, not clear how relevant is a relevant parameter at a given scale of operation.

It is known that the adhesion and surface energy [10,11] of  $\text{CF}_3$  terminated molecules are somewhat less than that of a  $\text{CH}_3$  terminated molecules although there appears to be some experimental evidence to the contrary [3,4]. In contrast, lateral force microscopy studies [1,2,5] clearly demonstrate that the friction corresponding to the former is significantly greater than that of the latter.

In moving to the backbone, it now appears established that molecular conformation has a profound effect on

\* Corresponding author. Tel.: +91 80 2293 2512/2351; fax: +91 80 2360 0648.

*E-mail address:* skbis@mecheng.iisc.ernet.in (S.K. Biswas).

tribological performance [9], with higher entropy and diminishing packing density [12,13] promoting higher friction. It is argued that this encourages additional channels of energy dissipation through the excitation of molecular motion [14,15]. A number of structural parameters such as atom size (fluorine is bigger than hydrogen) [1], chain length [14], lateral polymerizability [16], crystalline phase [2] and lattice parameters of the substrate material [17] influence the entropy and density of the molecular assembly. External variables, such as temperature [18] and pressure [19,20,12], influence adhesion and friction through their ability to influence the given structurally-determined entropy, this ability being itself a function of the a, priori structure [21]. In a boundary lubrication regime, as two mating asperities approach and move away from each other in an environment where energy is dissipated through friction, a molecule adsorbed on the substrate is subject to a thermal cycle. If the entropy is irreversible the next contact encounters a disordered assembly. We have concluded [22] on the basis of our studies of alkane thiols with different chain length ( $C_{18}$  and  $C_8$ ) that the potential for entropy change due to change in temperature is dependent on the a, priori defect density in the molecule. We have extended this approach here to two commercially available molecules; octadecyltrichlorosilane (OTS) [8] and 1H, 1H, 2H, 2H-perfluorooctyltrichlorosilane (FOTS) [7], which are potentially useful as boundary lubricants for aluminium and we have observed that the entropy generation is modest upto a heat treatment peak temperature of 483 K for OTS and 573 K for FOTS. FOTS is thus more thermally stable than OTS in spite of the latter being laterally polymerisable and of longer chain length (18 carbons) than the former (8 carbons). The OTS and FOTS differ not only by the fact that they are hydrogen and fluorine terminated respectively, but also the back bone in OTS has a zigzag configuration while that in FOTS has a helical structure.

In this paper we conduct tribological studies of FOTS and OTS in different regimes of normal load; 0–25 nN, 25–100 mN and 60 N (10 order load range), as a function of heat treatment cycle at different peak temperatures. The study is of immediate practical relevance as the test molecules are serious contenders for additive application in aluminium tribology. The rationale for this large span of test loads is however, not just to look for nano mechanical phenomena which in aggregate can explain macrotribology, but to establish different mechanisms which predominate different experimental scales. Today, practical processes are found at all scales, from nano to macro. The comparative study also provides us with a unique opportunity to observe the complex interplay of three basic, but not totally unrelated parameters, which are known to influence molecular tribology. FOTS adheres less than OTS, and this is known [9] to reduce friction.

It has a short chain compared to OTS which is known [22] to promote higher entropy and friction and finally it has a rigid rod like helical structure which may be suggested intuitively to offer greater resistance to sliding motion. We try to delineate each of these effects using a range of techniques; Atomic force microscopy (AFM), Fourier transform infrared (FTIR) spectroscopy, contact angle measurement, Surface enhanced Raman spectroscopy, contact force measurement, nanotribometry and macrotribometry and observe the predominant effects at room temperature and in situations where we control the molecular entropy by changing the heat treatment peak temperatures.

## 2. Experimental

### 2.1. Materials

Polycrystalline aluminium containing 97.25% aluminium, 1% silicon, 0.6% magnesium, 0.5% manganese and 0.35% iron is used as substrate. OTS and FOTS were purchased from Lancaster, UK and were used as received. Iso-octane (99.5%, dry) and *n*-hexadecane (99+%, anhydrous) obtained from Sd-fine-chem, India and sigma-Aldrich, USA, respectively were used as organic solvents. Deionised water, obtained by processing of distilled water through a Millipore purification system, was used to hydrolyse the aluminium substrate.

### 2.2. Sample preparation

Polycrystalline aluminium in strip (30×10×1.5 mm) and disc (10 mm diameter) dimensions were initially polished mechanically (sequentially with 1–3 and 0.25 μm diamond paste) to obtain 8–12 nm RMS (root mean square) roughness and then sonicated with acetone for 15 min to remove all polishing debris. The polished samples were kept in air for 1 h to generate a natural oxide film and then samples were sonicated with Millipore water for 30 min. Finally, the substrate was dried in a stream of dry nitrogen gas for 15 min and preserved in a desiccator. Before SAM deposition, samples were kept in a UV cleaning chamber for 30 min to burn off all carbonaceous contaminations, which would block adsorption sites. The aluminium samples, prepared as above, were immersed in freshly prepared additive solution (1 mM) for 1 h, taken out, rinsed and washed with iso-octane (twice) for 10 min to remove excess and physisorbed silane molecules. Finally the samples were kept in vacuum for 2 h.

### 2.3. FTIR analysis

All spectra were taken using Infra-Red Reflection Absorption Spectroscopy (IRRAS) on a Perkin Elmer GX

spectrometer equipped with a liquid nitrogen cooled Mercury Cadmium Telluride (MCT) detector. All the IR spectra reported here were referenced to bare aluminium substrate over 712 optimized scans at  $4\text{ cm}^{-1}$  resolution by using p-polarized beam. The sample chamber and detector were purged with nitrogen gas before starting the experiments and at regular intervals. A heating accessory (Harrick Scientific Corporation, New York, USA) was used for taking the spectra at different temperatures. When using the heating accessory, the infrared beam was reflected from the surface at an angle of  $75^\circ$  from the surface normal. The spectral analyses were carried out using Spectrum V 3.02 software from Perkin Elmer.

#### 2.4. Surface-enhanced Raman spectroscopy (SERS)

All spectra were taken by a RFS-100/s FT-Raman spectrometer (Bruker, Germany) equipped with a liquid nitrogen cooled Ge detector. All SERS spectra reported here were collected at room temperature after heat treatment of the samples with averaging of 1024 scans at  $1\text{ cm}^{-1}$  resolution.

#### 2.5. Contact angle measurement

The sessile drop contact angle ( $\theta$ ), measurements of SAMs was performed with Millipore water and methylene iodide using a Rame Hart Model 100-00 contact angle goniometer. The reported contact angle values are averaged over 10 separate measurements. An autopipetting system was used to control the amount of liquid ( $2\ \mu\text{L}$ ) placed for every measurement.

#### 2.6. Surface free energy

An approximate estimate of the surface free energy values obtained by resolving the resultant surface energy into contributions from the dispersion and dipole hydrogen bonding force components [23]. It is based on the measurement of contact angles with water and methylene iodide.

By measuring  $\theta$  for the two different liquids ( $\text{H}_2\text{O}$  and  $\text{CH}_2\text{I}_2$ ) against the SAM substrate, simultaneous equations are obtained which can be used to solve for  $\gamma_{\text{sv}}^{\text{d}}$  and  $\gamma_{\text{sv}}^{\text{h}}$ .

$$1 + \cos \theta = 2\sqrt{\gamma_{\text{sv}}^{\text{d}} \left( \frac{\sqrt{\gamma_{\text{lv}}^{\text{d}}}}{\gamma_{\text{lv}}} \right)} + 2\sqrt{\gamma_{\text{sv}}^{\text{h}} \left( \frac{\sqrt{\gamma_{\text{lv}}^{\text{h}}}}{\gamma_{\text{lv}}} \right)}$$

$\theta$  = contact angle of water or methylene iodide.

$\gamma_{\text{sv}}^{\text{d}}$  = surface energy of the surface from dispersive force component.

$\gamma_{\text{sv}}^{\text{h}}$  = surface energy of the surface from hydrogen bonding force component.

$\gamma_{\text{lv}}^{\text{d}}$  = surface energy of the liquid from dispersive force component ( $\gamma_{\text{lv}}^{\text{d}} \text{H}_2\text{O} = 21.8$  and

$$\begin{aligned} \gamma_{\text{lv}}^{\text{d}} \text{CH}_2\text{I}_2 &= 49.5\text{ mJ/m}^2). \\ \gamma_{\text{lv}}^{\text{h}} &= \text{surface energy of the liquid from hydrogen} \\ &\quad \text{bonding force component } (\gamma_{\text{lv}}^{\text{h}} \text{H}_2\text{O} = 51.0 \\ &\quad \text{and } \gamma_{\text{lv}}^{\text{h}} \text{CH}_2\text{I}_2 = 1.3\text{ mJ/m}^2). \\ \gamma_{\text{lv}} &= \text{free energy between liquid and vapor interface} \\ &\quad (\gamma_{\text{lv}} \text{H}_2\text{O} = 72.8 \text{ and } \gamma_{\text{lv}} \text{CH}_2\text{I}_2 = 50.8\text{ mJ/m}^2). \end{aligned}$$

and the sum of the components of the surface free energy will give the total solid surface free energy  $\gamma$ .

$$\gamma = \gamma_{\text{sv}}^{\text{d}} + \gamma_{\text{sv}}^{\text{h}}$$

#### 2.7. Adhesion and LFM measurement

All AFM experiments were performed using an ‘EXPLORER’ (Thermo Microscopes, Santa Barbara, USA), with  $\text{Si}_3\text{N}_4$  cantilevers (Thermo Microscopes) that have a pyramidal tip with a nominal end-radius of 30 nm. The cantilever normal stiffness was found using a thermal vibration technique inbuilt within the software. A V-shaped cantilever of stiffness 0.1 N/m was used for all experiments and was used to measure normal and lateral forces in (see Appendix A for detail). All tips were cleaned using a UV-cleaner (Bioforce Nanosciences, USA) for 20 min before use. Pull-off force and lateral force measurement were carried out in dry air (nominally 0% RH) (a custom made air tight humidity chamber was used) as well as in Millipore water. The sensors were calibrated by performing force curves on freshly cleaved mica. Deflections were recorded as a function of piezo movements during both approach and retraction; all adhesion experiments were performed in a peak load range of 0–20 nN. These deflections were then converted into force-separation curves. 250–300 measurements were made in each medium. An average value of the pull-off force with a standard deviation is reported here. For frictional force measurement, we examined both forward and reverse lateral force images ( $1\ \mu\text{m} \times 1\ \mu\text{m}$ ), recorded at different loads (0–25 nN). For roughness measurements, the scanner was allowed to attain stability before imaging. The imaging was carried out under ambient conditions with a high PID gain. We have used LFM images to obtain the 2D Fourier Transform (FFT) power spectra of the test molecules. The geometric symmetry of spots in the spectra reveals the crystalline symmetry of the molecule in SAM. We have used the FFT spectra to construct the atomic scale images of the terminal end of the molecules.

#### 2.8. Stiffness measurement

We used a dual double cantilever based on the ‘surface force’ type apparatus for contact stiffness measurements (for details see Ref. [24,25]). This is designated as contact force apparatus. It consists of two parallel and coaxial dual double cantilevers, in which one carries a spherical ruby probe (radius: 1.12 mm) and other carrying the SAM-coated

aluminum substrate. We compress the monolayer placed on a flexible platform, vibrate the pressing probe sinusoidally at sub-resonance frequency of 5 Hz and sub-nanometric amplitude of 0.5 nm and record the dynamic response of the platform. Using a visco-elastic model, the stiffness of the SAM was deconvoluted.

### 2.9. Nanotribometer

Tribological experiments were carried out in the range 25–100 mN using a nanotribometer (CSM Instruments, Switzerland). The nanotribometer is composed of three stepper motors (two in *X*- and *Y*-axis linked to pin-on-disc module and one in *Z*-axis linked to measuring head). The cantilever (removable) associated with two optical sensors for measurements of normal and lateral deflection was mounted on the measuring head. A 2 mm diameter 100 Cr6 steel ball is attached to the end of the cantilever. Before attachment, the steel ball was cleaned in acetone using an ultrasonic bath. Two optical sensing mirrors near to the cantilever head, perpendicular to each other (*X*- and *Z*-axis), measures the displacement of the cantilever during sliding against a SAM-coated aluminium disc. The friction coefficient was determined during sliding by measuring the deflection of the elastic arm of the cantilever in both horizontal and vertical planes with two high precision displacement sensors. All measurements were carried out

under ambient conditions (relative humidity: 42%, temperature: 295 K). The sliding speed was kept at 1 mm/s.

### 2.10. Macrotribometer

Macrotribological tests were carried out using a pin-on-disc machine, procured from DUCOM (Bangalore, India). The flat face of a high speed steel pin (diameter 3 mm) was loaded normally (60 N) and pressed against the flat surface of a rotating disc. An aluminium disc was slid against the pin at 0.2 m/s surface speed. The friction force was measured by a load cell attached to the pin holder (resolution 0.1 N) and the displacement of the pin was measured using a Syscon displacement sensor (LVDT, resolution 1  $\mu$ m). After each experiment the profile of the wear track was recorded using a profilometer (Talysurf, Taylor Hobson, Leicester, UK) and an average wear depth was calculated by estimating the integral area contained in the wear track and dividing it by the width of the track. *n*-Hexadecane was used as base oil and dispersed with 5% (v/v) of OTS and FOTS separately. Prior to the actual experiment a full pin-on-disc contact was established by running in; load 5 N speed 50 rpm. For the lubricated test, a drop of oil dispersed with the additives was placed at the interface, the normal load applied, and the test commenced. The tests were conducted for 250 m sliding distance.

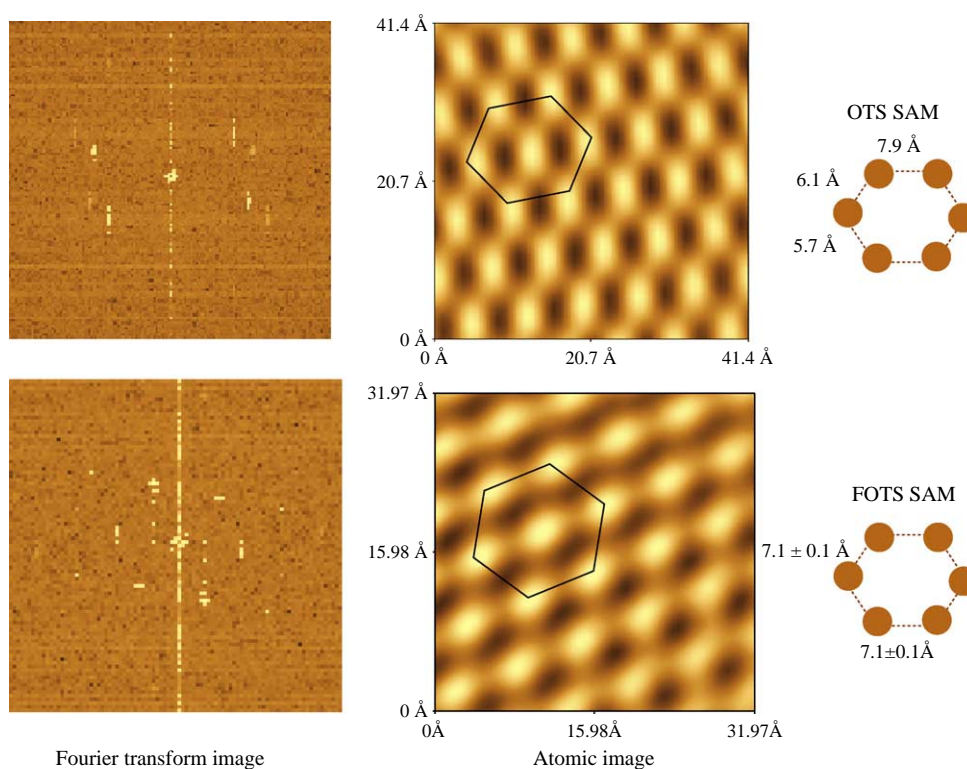


Fig. 1. Frictional force images for OTS and FOTS SAM on mica with their FFT image. There is no regular order in OTS SAM, however, FOTS SAM exhibits a regular hexagonal lattice with a lattice constant =  $7.1 \pm 0.1$  Å.

### 3. Results

#### 3.1. Characterization of self assembled monolayers

Fig. 1 shows lateral force images of FOTS and OTS self assembled on mica and the corresponding Fourier transform spectra. FOTS displays regular hexagonal symmetry in the Fourier transform spectrum in contrast to OTS SAM, where no long range order is observed and which indicates that FOTS SAM at room temperature is more ordered with a lattice constant of  $7.1 \pm 0.1 \text{ \AA}$  compared to that of the OTS. Fig. 2 shows peak frequency shift of methylene antisymmetric stretch, obtained from FTIR spectra taken during heat treatment of the SAM to different peak temperatures. We have noted desorption of OTS [8] and FOTS [7] at peak temperatures above 483 K and 573 K, respectively. The peak frequency shifts indicate that the residual disorder in the molecular backbone after a thermal cycle increases steadily with heat treatment peak temperature for OTS. For FOTS there is no residual disorder after heat treatment at a temperature of about 423 K. At higher temperature the residual disorder

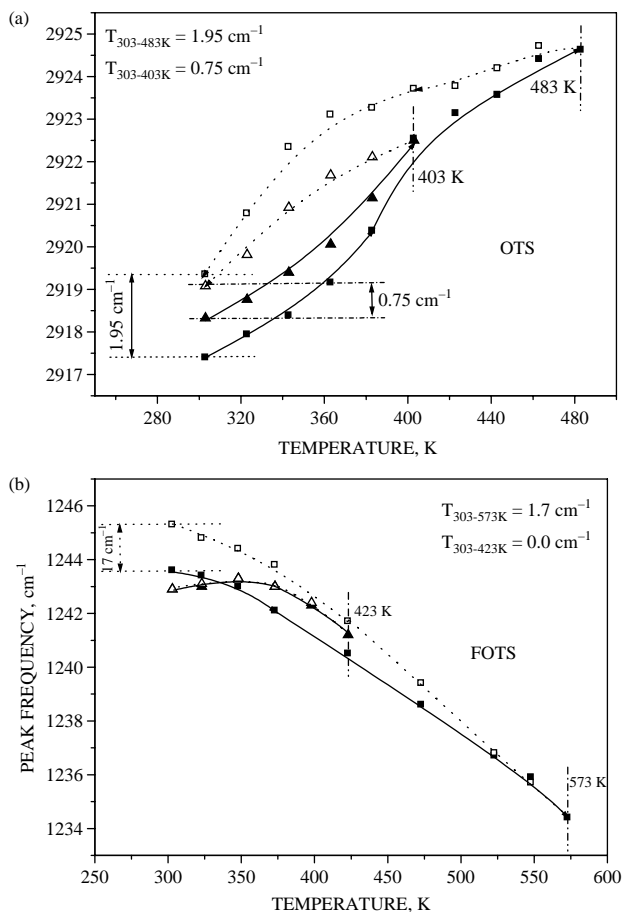


Fig. 2. Temperature dependence of peak frequency for different thermal cycles. (a) CH<sub>2</sub> antisymmetric stretch for OTS SAM on aluminium. Peak temperatures in the cycles are (■) 483 K and (▲) 403 K. (b) CF<sub>2</sub> antisymmetric stretch for FOTS SAM on aluminium. (■) 573 K and (▲) 423 K. Filled symbol is for heating and open symbol is for cooling.

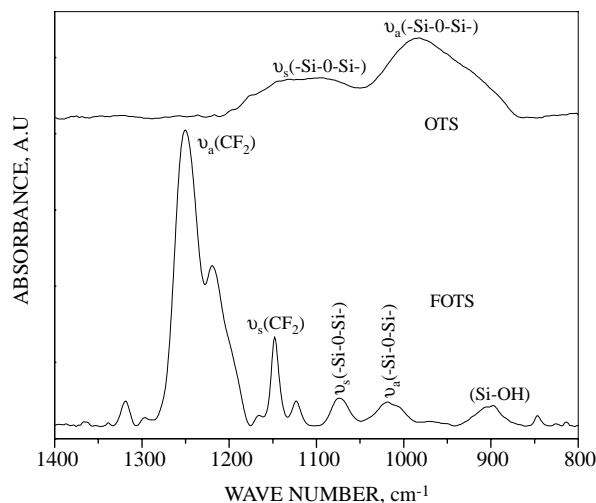


Fig. 3. FTIR spectra of OTS and FOTS SAM. In OTS spectra two bulk peaks (fused to each other) due to  $-\text{Si}-\text{O}-\text{Si}-$  antisymmetric and symmetric stretch ( $1072$  and  $982 \text{ cm}^{-1}$ , respectively) indicating presence of siloxane network, however, in FOTS same peaks are very weak ( $1074$  and  $1018 \text{ cm}^{-1}$ ). In addition, the presence of a  $\text{Si}-\text{OH}$  ( $897 \text{ cm}^{-1}$ ) peak indicates a low degree of polymerization in FOTS SAM.

increases, albeit more gradually than in the case of OTS, with peak temperature. Fig. 3 shows strong siloxane ( $-\text{Si}-\text{O}-\text{Si}-$ ) peaks at  $1072$  and  $982 \text{ cm}^{-1}$  (antisymmetric and symmetric stretch, respectively) for the OTS but for FOTS these peaks are very weak and also shows a silanol peak at  $897 \text{ cm}^{-1}$ . This indicates cross polymerization [8] of silanol group across the surface to result in a two dimensional  $\text{Si}-\text{O}-\text{Si}$  network in OTS SAM. Cross polymerization provides a constraint in the form of  $\text{Si}-\text{O}-\text{Si}$  link with bond length of  $\approx 3 \text{ \AA}$  [26] which is significantly less than the equilibrium distance of  $\approx 4.7 \text{ \AA}$  between the two adjacent alkyl chains. The steric hindrance imposed by the alkyl chain leads to molecular disorder as reflected by the inability [8] of the molecule to form three-dimensional networks. There is only a low degree of such polymerization in FOTS; the result is an ordered crystalline structure as seen in Fig. 1.

#### 3.2. Surface free energy and adhesion

Fig. 4 shows the surface free energy of the SAMs obtained from contact angle measurements as a function of heat treatment temperature. The order of surface energy at room temperature corresponds well to what has been found by others [10,11]. This reported trend of a hydrogen-terminated molecule exhibiting a higher surface free energy at room temperature (Fig. 4) than that for a fluorine-terminated molecule is in agreement with earlier results [11] but is also supported by pull-off measurements in AFM experiments [10] and our results obtained in dry air (nominally 0% RH) environment and in water as shown in Figs. 5 and 6. The surface free energy and adhesion of alkanethiol molecules assembled on gold increases on heat treatment with heat treatment peak temperature in dry

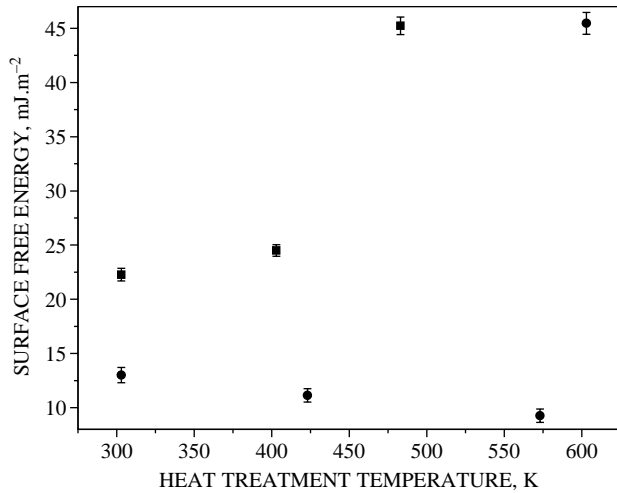


Fig. 4. Surface free energy of SAMs after heat treatment at different peak temperatures for (■) OTS and (●) FOTS, obtained from contact angle measurements.

conditions and decreases with heat treatment peak temperature in water medium is documented [27]. These effects are attributed to increases in molecular entropy due to heat treatment, the residual entropy after a heat treatment cycle increases with increasing peak temperature in the cycle. The OTS SAM in Fig. 4 shows an unambiguous increase in surface free energy with heat treatment peak temperature. This is not too surprising as Fig. 2 shows a steady increase in residual disorder due to heat treatment as the peak temperature is increased. For the thermally stable FOTS, the temperature-induced disorder is minimal and we see in Fig. 4, a modest change in free surface energy with heat treatment peak temperatures. While this difference between OTS and FOTS is partly understandable as the rate of defect accumulation with peak temperature is much greater for OTS than for the FOTS, the difference between the surface free energy and adhesion characteristics as seen in Figs. 4–6 for FOTS is not so easy to explain. We have probed this further using Surface Enhanced Raman Spectroscopy (SERS) and find the disorder for FOTS to decrease when heated from room temperature (Fig. 7) to 423 K, and then to increase between 423 and 573 K to a level higher than at room temperature. We would therefore, according to these data, expect a substantial increase in disorder when the FOTS SAM has been heated to 573 K. SERS data gives the shift in the peak frequency of the CF<sub>2</sub> rocking mode vibration and is therefore perhaps able to describe the state of the assembly at a microscopic scale better than the surface energy data which is a macroscopic thermodynamic quantity. Caution should therefore be exercised in the use of contact angle information to deconvolute microscopic tribological processes. Except for the adhesion results (Fig. 5a) of OTS at 0% RH, which do not show an unambiguous trend with peak temperature due to large experimental scatter, Figs. 5 and 6 show definite trend in adhesion between molecules at 0% RH and in water as well

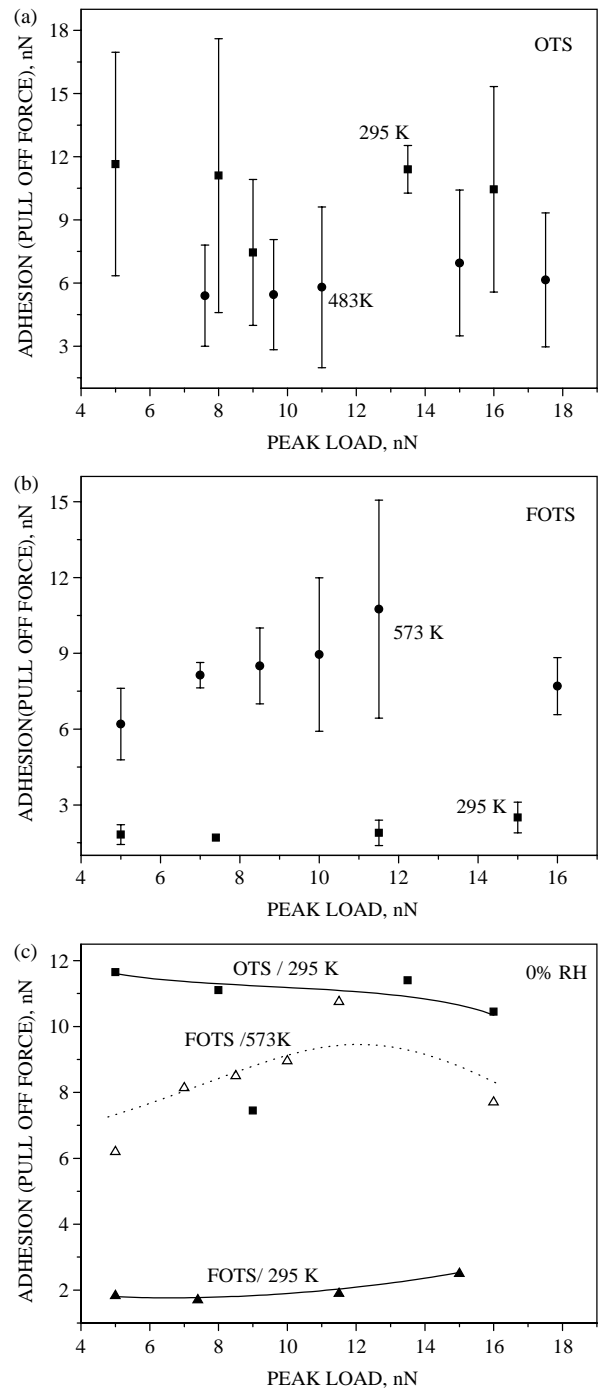


Fig. 5. Pull-off force (AFM) at different peak loads in dry air (0% RH) (a) OTS SAM; heat treatment temperatures (■) 295 K and (●) 483 K, (b) FOTS SAM; heat treatment temperatures of (■) 295 K and (●) 573 K and (c) Comparison of mean pull off force for (■) OTS and (▲) FOTS SAM at temperature 295 K and same open symbols for heat treatment temperature of 573 K, respectively. The data for OTS at 483 K are not shown due to large scatter in experimental data. Bar shows standard deviation ( $\pm\sigma$ ) of experimental scatter.

as when SAMs are heat-treated. Notwithstanding the large scatter in data, we have observed in the AFM pull off force measurements we may suggest the following trends with some confidence. In summary:

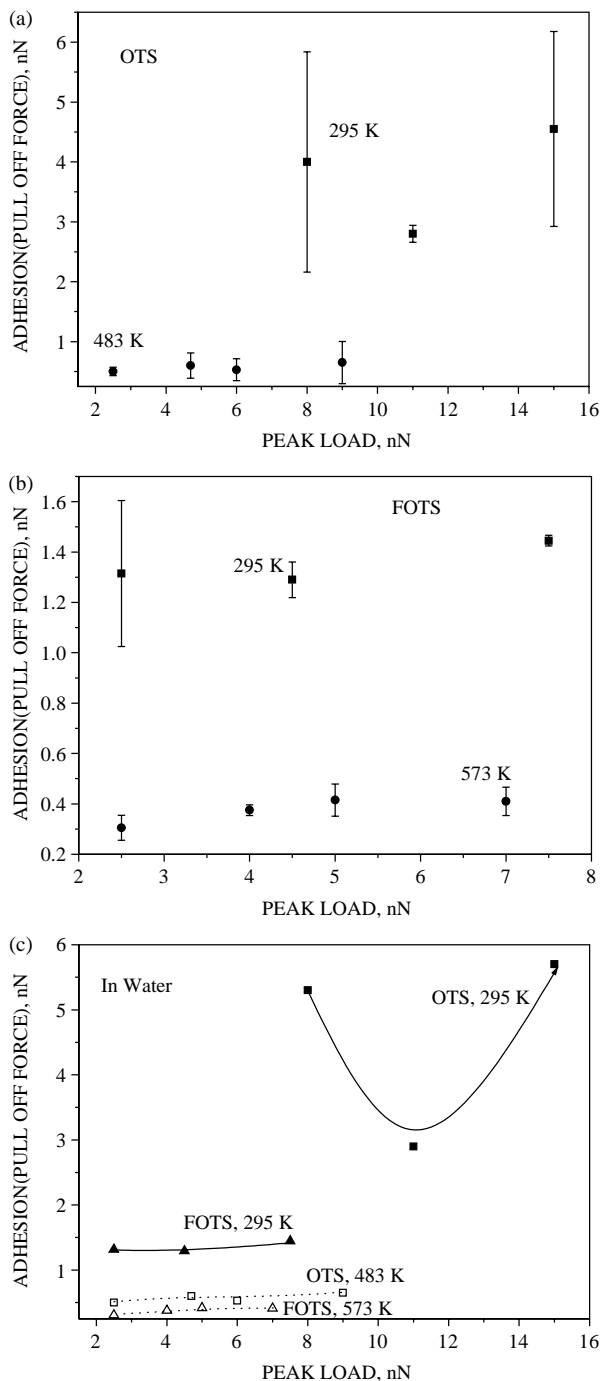


Fig. 6. Pull off force (AFM) at different peak loads in water (a) OTS SAM; heat treatment temperatures of (■) 295 K and (●) 483 K, (b) FOTS SAM; heat treatment temperatures of (■) 295 K and (●) 573 K and (c) Comparison of mean pull off force for (■) OTS and (▲) FOTS SAM at temperature 295 K and same open symbols for after heat treatment temperature of 483 K and 573 K, respectively.

1. The adhesion of FOTS at room temperature in 0% RH is always lower than that of OTS (Fig. 5c). We attribute this to the fact that OTS at room temperature is more disordered than the FOTS and therefore has a higher surface energy than that for the FOTS (Fig. 4).

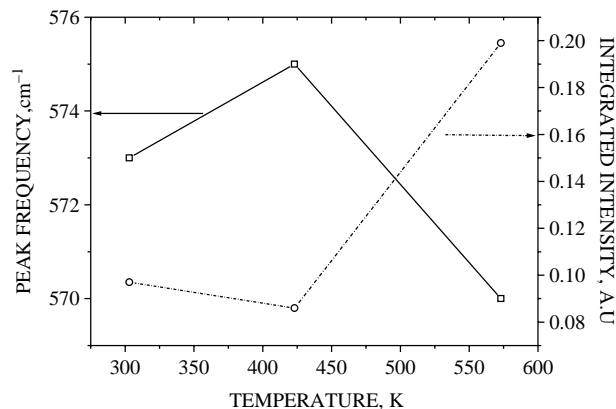


Fig. 7. Temperature dependence of CF<sub>2</sub> rocking vibration; peak frequency (□) and integrated intensity (○), measured by Surface Enhanced Raman Spectroscopy.

- The adhesion of FOTS at 0% RH increases with heat treatment peak temperature (Fig. 5b). For OTS, large experimental scatter denies an unambiguous conclusion. For FOTS the residual disorder (Fig. 2b) on heat treatment increases with peak temperature. While the corresponding surface energy data by contact angle measurements is ambiguous the SERS data indicates an increase in surface energy with increasing heat treatment peak temperature.
- The adhesion of both the molecules in water always decreases with increasing heat treatment peak temperature (Fig. 6a and b).
- The adhesion of all molecules at both the test peak temperatures in water medium is lower than that in 0% RH (Figs. 6c and 5c). This effect is well documented [28,29]. An unambiguous explanation of the effect still eludes us, the reported literature suggests that higher molecular disorder brought for example by heat treatment or reduction in chain length results in the terminal group increasingly attracting water molecules towards the SAM surface, giving rise to the formation of hydration layers [30] or interdigitation [31] into the backbone, both such effect would tend to reduce the force of adhesion. These are strong effects compared to the modulation of van der Waals force between the two interacting surfaces induced by a medium.

### 3.3. Lateral forces and friction

Moving now to molecular level friction obtained using the LFM it is clear that the surface free energy trends (Fig. 4) observed for each molecule with heat treatment peak temperatures and the adhesion trends (Figs. 5 and 6) for a test molecules are reflected faithfully in the corresponding lateral force characteristics (Figs. 8 and 9). The lateral forces recorded for FOTS, however, unlike the adhesion recorded for FOTS (Figs. 5 and 6), is always higher than that for OTS. These trends have also been

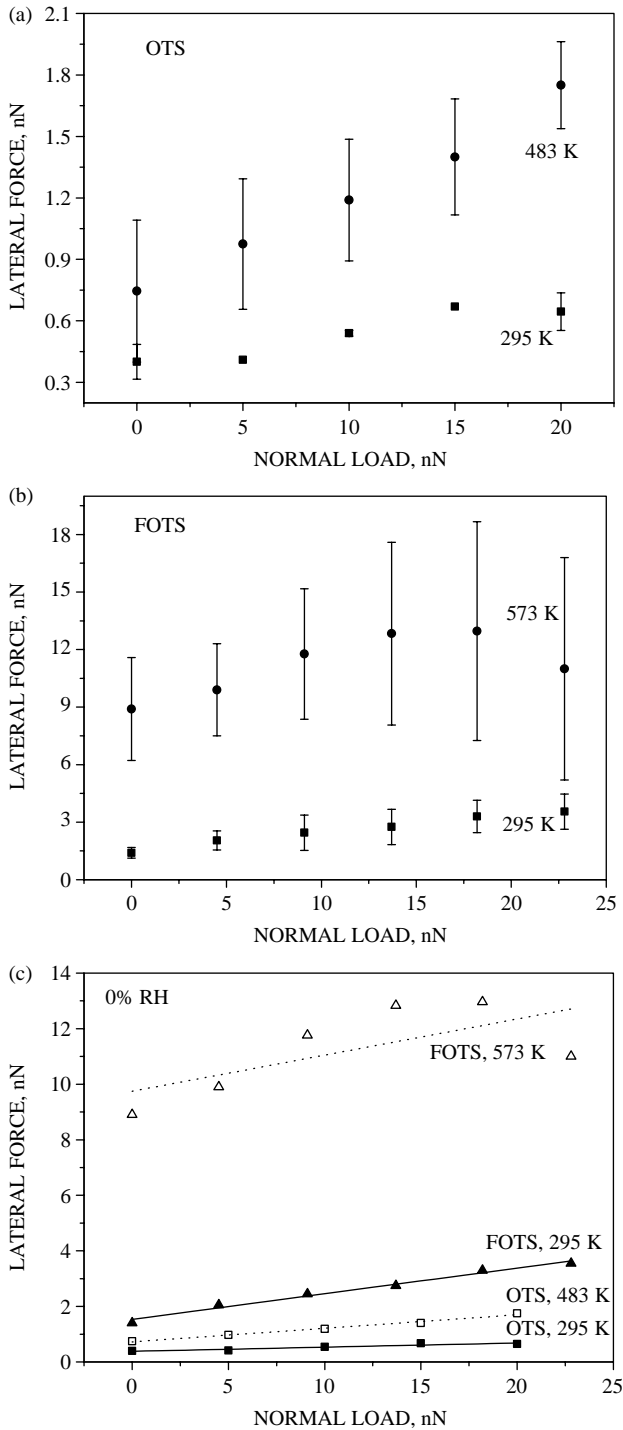


Fig. 8. Lateral force measurements taken at different normal loads in dry air (0% RH) (a) OTS SAM; heat treatment temperatures of (■) 295 K and (●) 483 K (b) FOTS SAM; heat treatment temperatures of (■) 295 K and (●) 573 K and (c) Comparison of mean lateral force for (■) OTS and (▲) FOTS SAMs at 295 K and same open symbols for heat treatment temperatures 483 K and 573 K, respectively.

recorded by others [1,2,11,32,33]. It is perhaps important to point out at this stage the fact that FOTS registers less adhesion (Figs. 5 and 6) than OTS and does not change with the medium of interaction (the trends are only different with

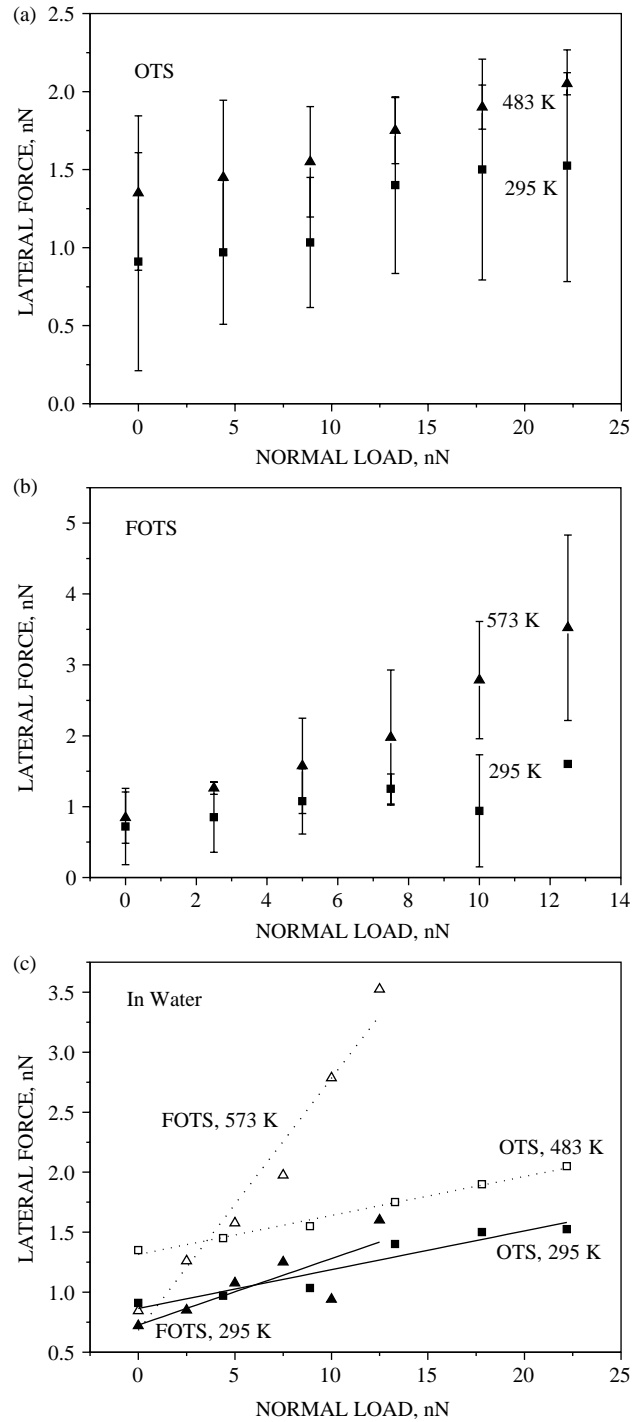


Fig. 9. Lateral force measurements taken at different loads in water (a) OTS SAM; heat treatment temperatures of (■) 295 K and (●) 483 K (b) FOTS SAM; heat treatment temperatures of (■) 295 K and (●) 573 K and (c) Comparison of mean lateral force for both (■) OTS and (▲) FOTS SAMs at 295 K and same open symbols for heat treatment temperatures of 483 K and 573 K, respectively.

respect to peak temperature). In lateral force microscopy (Figs. 8 and 9) the magnitude of the forces recorded are brought down significantly when the tests are done in water, but the principle differences between the response of the two

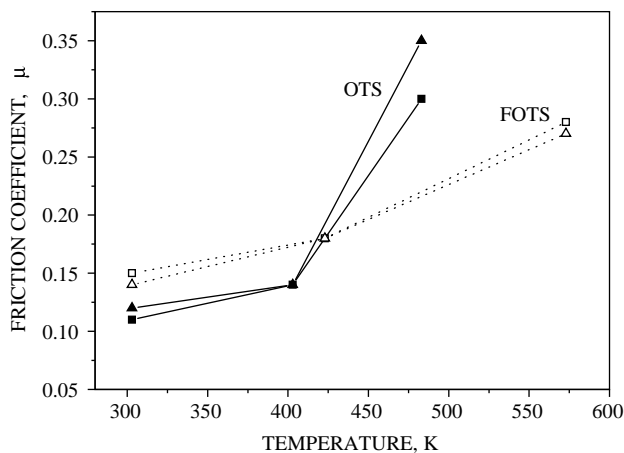


Fig. 10. Comparison of mean friction coefficient (obtained using a nanotribometer) of OTS and FOTS SAM on aluminium against steel ball after heat treatment, at two different loads. (■) 50 mN and (▲) 100 mN. Speed: 1 mm/s. Filled symbol is for OTS and open symbol is for FOTS SAM.

molecules recorded at 0%RH remain more or less unchanged when the experiments are performed in water. What is of great interest is to compare the Nanotribometry data for these test molecules. Fig. 10 shows that upto about 423 K the FOTS SAM registers a higher friction than OTS in conformity with the LFM data. For both molecules the friction coefficient increases steadily with heat treatment peak temperatures, a trend again in conformity with the LFM data. At 483 K, the OTS SAM registers a much higher friction than the FOTS SAM. Fig. 11 shows the wear resistance of the two SAMs. The FOTS SAM registers a greater wear resistance than the OTS SAM at all peak temperatures.

### 3.4. Macro-tribometry

Increasing the normal load by a further three orders (from nanotribometry) to perform macro-tribological tests (pin-on-disc), we note in Fig. 12 that the relative performance of OTS and FOTS is similar to what has been observed in Lateral Force Microscopy and Nanotribometry tests. We note that OTS additive gives rise to more wear compared to that observed for FOTS (Fig. 12b), however, OTS register low friction compare to FOTS (Fig. 12a). Here, the macrotribometry tests were performed with the test molecules dispersed in *n*-hexadecane oil.

## 4. Discussion

We have performed a series of tribological tests in different regimes of load spanning 10 orders ( $10^{-9}$ –10) of magnitude to elucidate the difference in tribological performance between two molecules; namely FOTS and OTS. Our work shows that the difference between these

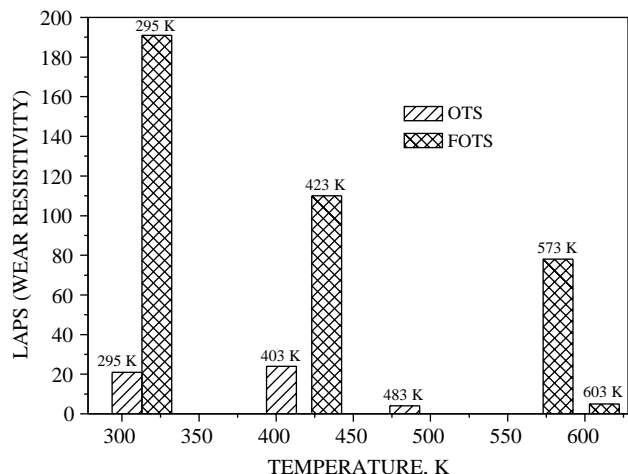


Fig. 11. Comparison of wear resistivity of OTS and FOTS SAM on aluminium against steel ball after heat treatment. Load: 100 mN, speed: 1 mm/s. Line bar is for OTS and cross bar is for FOTS SAM. The wear resistivity is the number of laps (revolutions of the disc) taken for the coefficient of friction to equal that of the steel ball against the bare substrate.

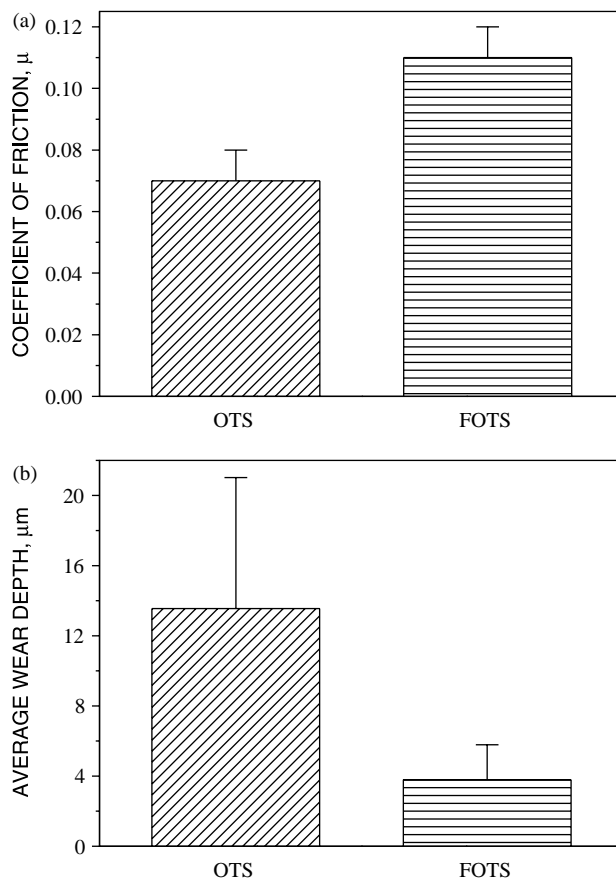


Fig. 12. (a) Coefficient of friction of aluminum against steel pin in presence of OTS and FOTS additives (5% v/v) dispersed in *n*-hexadecane. (b) Wear measurement of aluminum against steel pin in the presence of OTS and FOTS additives for 250 m sliding distance. Load: 60 N, speed: 0.2 m/s.

molecules in terms of surface free energy obtained from contact angle measurement is reproduced qualitatively by the adhesion data acquired from AFM experiments performed in dry air (0% RH) and water. When lateral forces were measured in the AFM, at the same scale of contact and the order of normal load, as those used to obtain the force curves for adhesion force, the trend is, however, completely reversed. In contrast to the adhesive forces for FOTS being less than those for OTS, the lateral forces for FOTS are found to be greater than those measured for OTS. This trend reversal between the test molecules is also found when sliding experiments were performed in a nanotribo-meter in the ambient conditions, at normal loads (25–100 mN) which are six orders of magnitude greater. We first note that the attraction between the  $\text{Si}_3\text{N}_4$  tip in AFM and the OTS is more attractive than that between the same tip and the FOTS. This coupled with the fact that the OTS SAM is more disordered and therefore more hydrophilic than the FOTS accounts for the trend in surface energy and adhesion. As per our present understanding [9], both these effects should yield at least at room temperature, higher frictional forces for the OTS than for the FOTS.

The molecular level mechanisms of friction suggested by previous works fall into four groups.

1. Adhesion at the terminal group level [9,30].
2. Dissipation opportunities provided by molecular disorder [13,15,32,34] and/or coherence length related to packing density and size of terminal groups [33].
3. Resistance to translational and rotational movement of the molecules in the assembly [33,2,5]. Rotational movement about the molecular axis or a bond axis generates gauche defects. The gauche defect population is determined by temperature [22] and pressure [21]. Thus when a molecule is bent like a cantilever to accommodate tangential motion, the resistance may be accounted for by the resistance to tilt as well as to the generation of gauche defects. Considering that the stiffness of a system is a product of elastic modulus and a length scale related to contact area, we assign an aggregate term ‘molecular stiffness’ which expresses the total resistance to tangential motion. The product of such a stiffness and tangential displacement gives the friction force.
4. Molecular level roughness [1].

Clearly the mechanisms listed above are not totally independent of each other and for a given molecular assembly changes in pressure, temperature or medium of interaction would tend to affect all of them to perhaps different extents. We contend that different mechanisms are dominant in different situations. We try to isolate the mechanism predominantly responsible for frictional difference between two molecules, pressure, temperature and medium remaining unchanged or between two thermal states of the same molecule.

We thus look at the frictional difference between FOTS and OTS SAMs on aluminium at room temperature. Kim et al. [33] have argued that the disorder in a fluorinated molecule is invisible in AFM imaging. This we discount as our FTIR, surface energy and adhesion data tend to support our AFM imaging data that FOTS is more ordered than the OTS. The other ‘coherence length’ argument of these workers to support the thesis that fluorinated molecules have more channels of energy dissipation may indeed be true, but without any direct experimental validation, cannot be accepted unequivocally. Thus notwithstanding this, we state that neither adhesion nor the molecular disorder of the systems can account (they may modulate) for the fact that when a steel ball slides against the FOTS SAM the friction is higher than when the same is done against the OTS SAM.

We therefore, turn to the ‘molecular stiffness’ concept by measuring it directly using a SFA type of apparatus [24,25]. Fig. 13 shows that the stiffness of a FOTS SAM is significantly higher than OTS SAM. We therefore, conclude that the frictional difference between these molecules at room temperature is significantly contributed to by their difference in stiffness. We also show in Fig. 13 the stiffness of more-ordered fluorinated molecules with 10 (rather than 8 in FOTS) carbon atoms in the backbone. Molecular order on the one hand at least at room temperature, does not appear to make a significant difference. On the other hand, the rigid rod like conformation of the helically-structured fluoro alkyl chain, as has been noted by others [2], appears to be the predominant influence which gives higher stiffness for FOTS than OTS and hence higher friction.

We now address the frictional properties of each test molecule with reference to the adhesive contribution to friction. Fig. 14 shows the frictional forces measured in

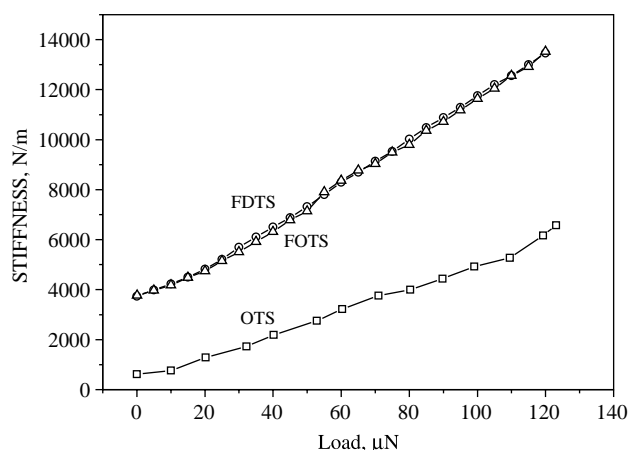


Fig. 13. Stiffness of OTS ( $\square$ ), FOTS ( $\circ$ ) and FDTS ( $\triangle$ ) on aluminium were measured on a contact force apparatus using an AC modulation technique. The measurements were carried out for an excitation amplitude of 0.5 nm at 5 Hz.

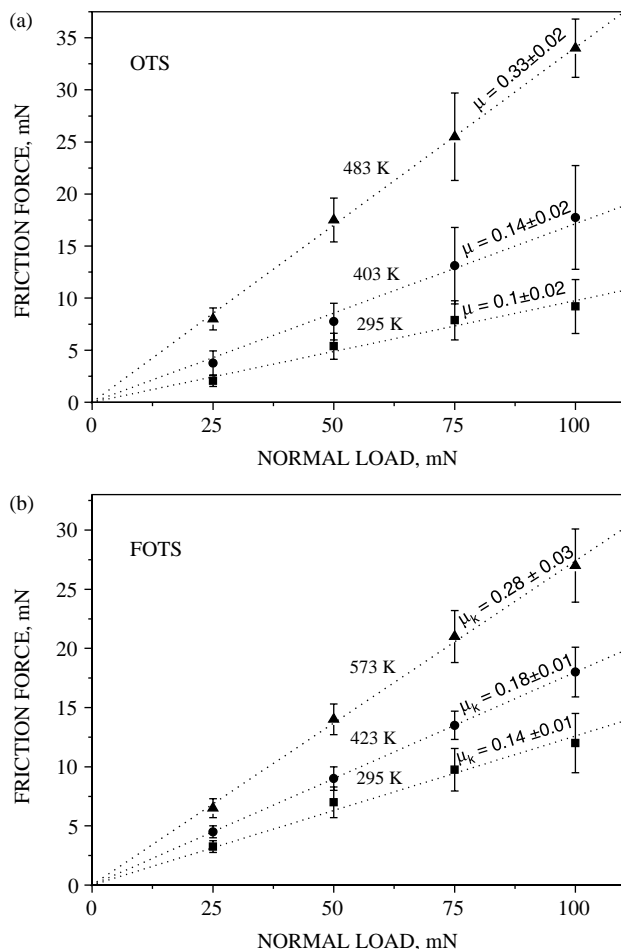


Fig. 14. Friction forces measured by using the nanotribometer at different loads for (a) OTS SAM after heat treatment, peak temperatures of (■) 295 K, (●) 403 K and (▲) 483 K. (b) FOTS SAM after heat treatment, peak temperatures of (■) 295 K, (●) 423 K and (▲) 573 K.

the nanotribometer as a function of normal load and heat treatment peak temperature. As the linear characteristics for both molecules converge to zero at 0 mN load we may conclude, with reference to a constitutive equation,

$$F = \mu(F_a + P)$$

( $F_a$  is the adhesive force and  $P$  is the normal load and  $\mu$  is the coefficient of friction), that within the force measurement resolution of the nanotribometer the adhesive force contributes negligibly to the friction force when the normal load is in the mN range. Adhesion, however, plays an important role when the adhesion and normal loads are in the same regime (we assume that the adhesive (pull off) force as per the JKR and DMT theories [35] is independent of load), as in the LFM experiments. We assume that there is an adhesion induced friction force  $\mu F_a$  (where  $F_a$  is an average value of pull off force recorded at 0% RH) (as per the DMT model [35]) does not change with normal load. We subtract the friction force due to adhesion,  $\mu F_a$ , from the

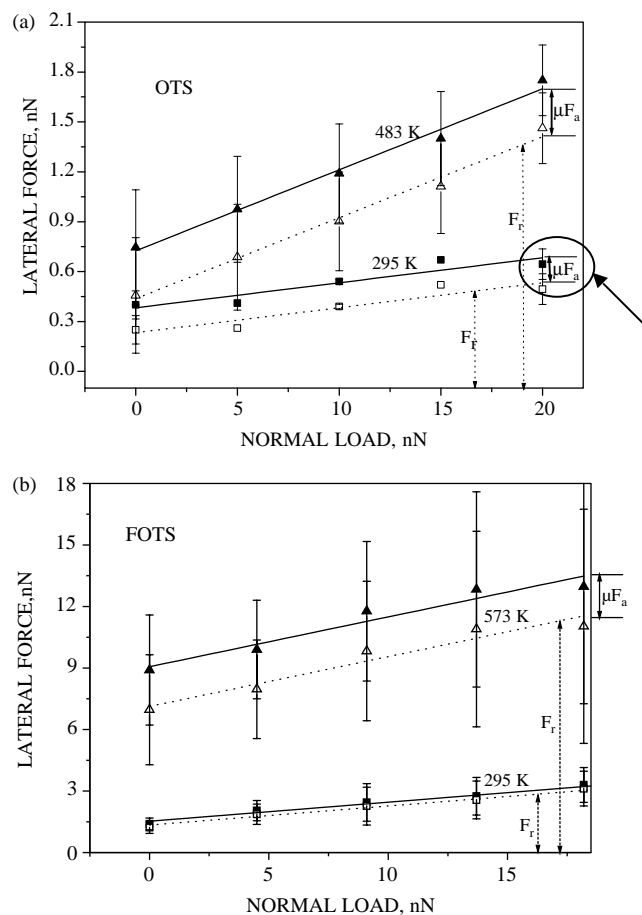


Fig. 15. Influence of adhesion on lateral force (in dry air, 0% RH); (a) total lateral force due to OTS SAM after heat treatment, temperatures of (■) 295 K and (▲) 483 K and residual friction force indicated by open symbol at same temperature and (b) Total lateral force due to FOTS SAM after heat treatment, temperatures of (■) 295 K and (▲) 573 K and residual friction force indicated by open symbol at same temperatures. Lateral force increases with heat treatment temperature; lateral force due to adhesion also increases with heat treatment temperature. The data is a repeat of what is given in Fig. 8 to analyses the contribution of adhesion on friction.

total lateral force  $F$  recorded and show in Fig. 15 that there is a residual friction force  $F_r$ , which increases when the heat treatment temperature is increased. If we now consider that  $\mu F_a$  arises primarily out of interactions at the terminal group level (we note that it is therefore important when the normal loads are small in the ranges), and the increase in adhesive component of this friction force, with increasing heat treatment temperature is due to increasing levels of disorder introduced at the terminal level, we can attribute the residual friction force  $F_r$  to bulk disorder and comment that  $F_r$  increases with temperature as increasing opportunities for energy dissipation materialize. What is, however, not clear from the lateral force measurement is whether the normal load also contributes to bulk disordering as has been suggested by Siepmann and McDonald [19] and Mikulski and Harrison [12]. This would be reflected in the slope of the friction force graph with load or the coefficient of friction.

Large scatter in the lateral force data prevents a definitive conclusion in this regard. We thus resort to the Nanotribometry data shown in Fig. 14. Here, in the absence of perceptible adhesion, we note an increase in the coefficient of friction with peak temperature. We have measured the stiffness of our test molecules heat-treated to different peak temperatures. For a given molecule, we find the stiffness to remain unchanged with peak temperature. Extending our discussion of the lateral force data we may thus conclude that it is not only the peak temperature, but also the normal load, which contributes to molecular disorder, enhancing opportunities for energy dissipation and therefore the friction force. To emphasize the point let us now compare the increase in friction force for FOTS (Fig. 14b) between 75 and 100 mN. The increase is significantly more when the heat treatment temperature is 573 K compared with when the temperature is 295 K. If the difference in friction force recorded at a normal load at different heat treatment peak temperatures is due to the difference in molecular order, our data (Fig. 14) shows clearly that the change in molecular order is also a function of normal load. If not, the friction force characteristics at different temperatures would be translated parallel to each other recording the same coefficient of friction.

Considering that the mean pressure obtained presently in macrotribometry is low (8.5 MPa) compared to what were experimented with in LFM and nanotribometry we may compare the macrotribometry data with that obtained in nanotribometry in the 300–423 K range. It is remarkable to observe that (a) in both cases FOTS register higher friction and better wear resistance than what are recorded for OTS (compare Fig. 12 with Figs. 14 and 11) and (b) the friction coefficients recorded in both cases are very similar. Considering that in macrotribometry the additive molecules dispersed in oil come to the contact only when vacant sites are available and in nanotribometry they are anchored as a self assemble monolayer once in for all, this identity between the results of the tests is most interesting. It therefore, leads us to conclude that in macrotribometry it is the self-assembly state of the molecules on a substrate, however, temporary, controls the tribological interactions. The results also point to the potential of a desktop nanotribometry as a screening test for additive molecules.

## 5. Conclusions

The tribological performance of two potential additives for the lubrication of aluminium is determined over a load range, which spans 10 orders of magnitude. At very low loads, the tribology of self-assembled monolayers on aluminium is much influenced by adhesion, which scales with molecular entropy. The friction, though influenced by entropy is also found to be sensitive to the mechanical stiffness of the molecules.

These observations hold when the load is increased by six orders of magnitude except that the effect of adhesion is marginalized. In interpreting the tribological data we conclude that the both temperature and pressure (order of  $\approx 225$ – $310$  MPa) influence molecular order and thereby dissipative avenues and friction. Macrotribological experiments with additive molecules dispersed in *n*-hexadecane (10 orders of load more than nano tribology) leads us to conclude that the self assembly state of the molecules on a substrate is temporary and only come in contact when vacant sites are available, controls the tribological interactions. Conformational order and molecular stiffness play an important roles to determine the tribological performance of the additive molecules to the reactive interface, and thereby friction and wear.

## Acknowledgements

The authors are grateful to General Motors (R&D), Warren, USA and the Centre for High Technology, Ministry of Petroleum, Govt. of India for the financial grant, which has made this work possible. They also acknowledge the help of Ms N. Prathima and Mr H.S. Shamasunder for carrying out this work.

## Appendix A. Cantilever calibration for normal and lateral force measurements

### A.1. A. Normal force conversion

From the AFM, slope of the force-distance curve in the repulsive region gives normal sensor response NR,

$NR = z(nA)/d(nm)$ ;  $z$  is deflection of cantilever (nA) and  $d$  is piezo displacement (nm)

The cantilever deflection in nA can be converted to nm,

$$z(nm) = \frac{z(nA)}{NR}$$

The normal force acting on the cantilever is given by

$$F_n(nN) = K_c z(nm)$$

where  $K_c$  is the stiffness of the cantilever as obtained from calibration and Finite Element Method estimation.

### A.2. B. Lateral force conversion

In LFM measurement, the cantilever probe moves perpendicular to the axis of the cantilever; friction force causes torque on the tip and twists the cantilever. The cantilever surface act as a mirror and when the cantilever twists, the angle of incidence and angle of reflection get changed. Therefore change in reflection angle changes response current of quadrant photo-sensitive diode (PSD). Hence the change in response current of PSD is actually

due to change in the reflection angle and is PSD sensitive to only the change in the laser spot on it. Therefore the sensitivity of the PSD due to change in the angle of reflection, is constant in all directions. Let us consider the length of the cantilever as ' $L$ ' and the height of the tip as ' $t$ '. Now we can write the angular response (AR) of the cantilever-photodiode arrangement as,

$$AR = \frac{z(nA)}{\frac{d(nm)}{L}} \quad \text{or} \quad AR = NR \times L(nA/\text{rad})$$

where  $d(nm)/L \approx \theta$  in radian is the angular deflection of the cantilever for the vertical deflection ' $d$ ' and NR is the normal response.

In the case of lateral force measurement, torque ' $T$ ' acting on the cantilever due to friction force  $F_f$  is given by,

$$T = F_f \times t$$

Let the twist angle be  $\phi$ , due to twist we get lateral response, 'LRA' from PSD in nA. The lateral response in nA can be converted to twist angle radians by

$$\phi(\text{rad}) = \frac{\text{LRA}}{\text{AR}}$$

Using finite element analysis we estimated  $C_2 = T/\phi$  for a cantilever, taking the dimension and material constants from the suppliers data specification sheet. Then the lateral force in nanoNewton is given by

$$F_f = C_2 \phi \frac{1}{t}.$$

## References

- [1] Sung I-H, Yang J-C, Kim D-E, Shin B-S. *Wear* 2003;255:808–18.
- [2] Takahara A, Kojio K, Kajiyama T. *Ultramicroscopy* 2002;91:203–13.
- [3] Hayashi K, Sugimura H, Takai O. *Appl Surf Sci* 2002;188:513–8.
- [4] Hayashi K, Sugimura H, Takai O. *Jpn J Appl Phys* 2001;40:4344–8.
- [5] Kojio K, Takahara A, Kajiyama T. *Langmuir* 2000;16:9314–20.
- [6] Clear SC, Nealey PF. *J Colloid Interface Sci* 1999;213:238–50.
- [7] Devaprakasam D, Sampath S, Biswas SK. *Langmuir* 2004;20:1329–34.
- [8] Khatri OP, Biswas SK. *Surf Sci* 2004;572:228–38.
- [9] Carpick RW, Salmeron M. *Chem Rev* 1997;97:1163–94.
- [10] Burnham NA, Dominguez DD, Mowery RL, Colton RJ. *Phys Rev Lett* 1990;64:1931–4.
- [11] Graupe M, Koini T, Kim HI, Garg N, Miura YF, Takenaga M, et al. *Colloids Surfaces A* 1999;154:239–44.
- [12] Mikulski PT, Harrison JA. *J Am Chem Soc* 2001;123:6873–81.
- [13] Yang X, Perry SS. *Langmuir* 2003;19:6135–9.
- [14] Lio A, Charych DH. M. Salmeron, *J Phys Chem B* 1997;101:3800–5.
- [15] McDermott MT, Green J-BD, Porter MD. *Langmuir* 1997;13:2504–10.
- [16] Granier M, Lanneau GF, Moineau J, Girard P, Ramonda M. *Langmuir* 2003;19:2691–5.
- [17] Lu W, Suo Z. *Phys Rev B* 2002;65:2054181–7.
- [18] Noy A, Zepeda S, Orme CA, Yeh YJ. *J Am Chem Soc* 2003;125:1356–62.
- [19] Siepmann JJ, McDonald IR. *Phys Rev Lett* 1993;70:453–6.
- [20] Barrera E, Ocal C, Salmeron M. *J Chem Phys* 2000;113:2413–8.
- [21] Tutein AB, Stuart SJ, Harrison JA. *Langmuir* 2000;16:291–6.
- [22] Prathima N, Harini M, Rai N, Chadrashekara RH, Ayappa KG, Sampath S, Biswas SK. *Langmuir* 2005;21:2364–74.
- [23] Owens DK, Wendt RC. *J Appl Poly Sci* 1969;13:1741–7.
- [24] Devaprakasam D, Biswas SK. *Rev Sci Instrum* 2003;74:1228–33.
- [25] Devaprakasam D, Biswas SK. *Rev Sci Instrum* 2005;76:0351021–0351027.
- [26] Stevens MJ. *Langmuir* 1999;15:2773–8.
- [27] Prathima N, Shankar N, Ayappa KG, Biswas SK. communicated to *J Colloid Interface Sci*.
- [28] Weisenhorn AL, Maivald P, Butt H-J, Hansma PK. *Phys Rev B* 1992;45:11226–32.
- [29] Kokkoli E, Zukoski CF. *J Colloid Interface Sci* 1999;209:60–5.
- [30] Warszynski P, Papastavrou G, Wantke K-D, Mohwald H. *Colloids Surfaces A* 2003;214:61–75.
- [31] Duwez A-S, Jonas U, Klein H. *Chem Phys Chem* 2003;4:1107–11.
- [32] Schonherr H, Vancso G. *J Mater Sci Eng C* 1999;8,9:243–9.
- [33] Kim HI, Koini T, Lee TR, Perry SS. *Langmuir* 1997;13:7192–6.
- [34] Xiao X, Hu J, Charych DH, Salmeron M. *Langmuir* 1996;12:235–7.
- [35] Johnson KL. *Contact mechanics*. Cambridge: Cambridge University Press; 2001.